PHYSICAL REVIEW B **92**, 220401(R) (2015)

Asymptotic freedom in quantum magnets

H. D. Scammell and O. P. Sushkov
School of Physics, The University of New South Wales, Sydney, New South Wales 2052, Australia
(Received 29 June 2015; published 2 December 2015)

Phase transitions in isotropic quantum antiferromagnets are described by an O(3) nonlinear quantum field theory. In three dimensions, the fundamental property of this theory is logarithmic scaling of the coupling constant. At the quantum critical point the coupling asymptotically vanishes, and the quasiparticles become free. This logarithmic decay of the coupling constant has never been observed. In this Rapid Communication, we derive finite-temperature properties of the field theory and use our results to analyze the existing data on the real antiferromagnet $TlCuCl_3$. Including finite temperatures in the theory, we find that agreement between theory and experiment is sufficiently sensitive to unambiguously identify the asymptotic decay of the coupling constant. We also comment on the unique possibility to study Landau pole physics in quantum magnets.

DOI: 10.1103/PhysRevB.92.220401 PACS number(s): 75.10.Jm, 64.70.Tg, 75.40.Gb

Asymptotic freedom plays a crucial role in quantum chromodynamics. The freedom, which is due to non-Abelian gauge fields, means a logarithmic decay of the coupling constant at high energies. Ultimately, at infinite energies particles do not interact; this is ultraviolet asymptotic freedom [1,2]. In three-dimensional (3D) nongauge quantum field theories as well as in Abelian gauge theories, the coupling constant decays logarithmically at low energies [3]. However, usually, this decay is terminated because of a low-energy cutoff. For example, in quantum electrodynamics the cutoff is due to the rest energy of the electron. The low-energy logarithmic decay can be observed only at a quantum critical point (QCP) where the cutoff energy is zero. Slightly overstretching the accepted terminology, we call this phenomenon "infrared asymptotic freedom." Three-dimensional quantum antiferromagnets in the vicinity of a QCP provide a perfect testing ground for such behavior. Like in QCD the effect is related to the dimensionality of the problem; it occurs only at the upper critical dimension (3D + time). Logarithmic running of the coupling is known in other condensed-matter systems too. For example, the Fermi velocity in graphene grows logarithmically at low energy [4]. This results in a logarithmic effective coupling constant [5]; however, unlike in field theory the quasiparticle dispersion is changing. A closer analogy to the present discussion is known in 1D spin systems, where the effective interaction between spinons logarithmically decays at low energy [6,7]. This, however, is unrelated to physics at the upper critical dimension.

The 3D quantum antiferromagnet $TlCuCl_3$ can be driven from a magnetically disordered to magnetically ordered phase by pressure [8]. This provides a unique opportunity to study the physics described above. The low-energy logarithmic behavior at a QCP can, in principle, be pinned down even at zero temperature [9]. The zero-temperature case is well understood theoretically; a 3D *quantum* antiferromagnet at zero temperature is equivalent to a four-dimensional (4D) *classical* antiferromagnet at finite temperature. The 3D QCP corresponds to the Néel transition in the 4D case. Thermodynamic quantities scale as powers of the running coupling constant [10]. Unfortunately, the existing zero-temperature experimental data are insufficient to pin down the logarithmic scaling. On the other hand combined zero and nonzero temperature data on $TlCuCl_3$ [11–13] provide an excellent opportunity to search for fingerprints of asymptotic freedom at the QCP. To perform this search we develop a theory of the QCP which accounts for both quantum and thermal fluctuations. After that we compare the theoretical predictions with experimental data. The comparison unambiguously indicates a logarithmically running coupling constant.

The phase diagram of the dimerized 3D quantum antiferromagnet $TlCuCl_3$ is shown in the vertical panel of Fig. 1. The disordered quantum state consists of an array of spin dimers (spin singlets), and the ordered quantum state has a long-range Néel order, as illustrated in Fig. 1. The Néel temperature curve (red line) separates ordered and disordered phases, with QCP indicated by a yellow dot.

Excitations in the disordered phase, triplons, are gapped. These are triplet excitations of spin dimers [Fig. 2(a)]. There are two kinds of excitations in the ordered phase: gapped longitudinal Higgs and gapless Goldstone excitations. They are illustrated in Figs. 2(b) and 2(c). The horizontal panel in Fig. 1 displays excitation gaps versus pressure at zero temperature.

Overall, the experimental data [11–13] provide the following information: (i) Néel temperature versus pressure, (ii) the magnetic excitation gap in the disordered phase for various temperatures and pressures, (iii) the Higgs magnon excitation gap in the antiferromagnetic phase for various temperatures and pressures, and (iv) the magnetic excitation width (lifetime) for various temperatures and pressures. In our analysis we do not use fully the width data; the width is used only to indicate the dimensional crossover region around the Néel temperature. However, we fully use the data from points (i), (ii), and (iii). There is a small spin-orbit anisotropy in $TlCuCl_3$ which gaps one of the "Goldstone" modes in the antiferromagnetic phase. This implies that the number of dynamic degrees of freedom changes from three at high energy to two at very low energy. We neglect this effect here, but in Supplemental Material Section E [14] we show that this effect does not influence our conclusions.

The quantum phase transition (QPT) between ordered and disordered phases is described by the effective field theory with the following Lagrangian [15–18]:

$$\mathcal{L} = \tfrac{1}{2}\partial_\mu\vec{\varphi}\partial^\mu\vec{\varphi} - \tfrac{1}{2}m_0^2\vec{\varphi}^{\,2} - \tfrac{1}{4}\alpha_0[\vec{\varphi}^{\,2}]^2. \qquad (1)$$

The vector field $\vec{\varphi}$ describes staggered magnetization, and index μ enumerates time and three coordinates. The QPT results

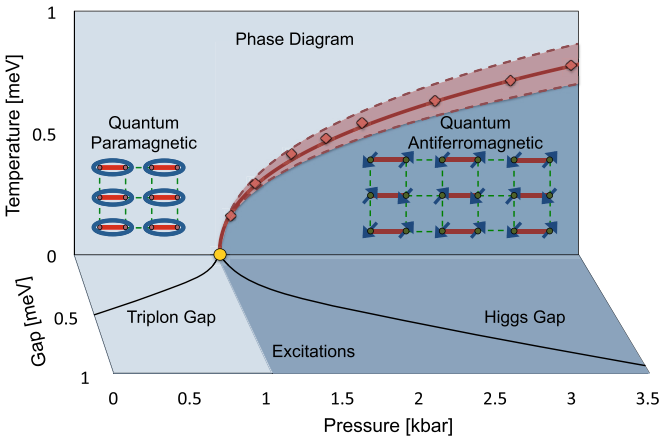

FIG. 1. (Color online) The phase/energy diagram of $TlCuCl_3$ [11]. The vertical panel shows the pressure-temperature phase diagram; the Néel temperature curve separates magnetically ordered and magnetically disordered phases. The light red band around the Néel curve indicates the region of dimensional crossover. The horizontal panel shows both the triplon gap Δ_t in the paramagnetic phase and the Higgs magnon gap Δ_H in the antiferromagnetic phase vs pressure at zero temperature.

from tuning the mass term m_0^2, for which we take the linear expansion $m_0^2(p) = \gamma^2(p_c - p)$, where $\gamma^2 > 0$ is a coefficient and p is the applied pressure. Varying the pressure leads to two distinct phases; (i) for $p < p_c$ we have $m_0^2 > 0$, and the classical expectation value of the field is zero $\varphi_c^2 = 0$. This describes the magnetically disordered phase; the system has a global rotational symmetry, and the excitations are gapped and triply degenerate. These excitations are referred to as "triplons." (ii) For pressures $p > p_c$ we have $m_0^2 < 0$, and the field obtains a nonzero classical expectation value $\varphi_c^2 = \frac{|m_0^2|}{\alpha_0}$. This describes the magnetically ordered, antiferromagnetic phase. Varying m_0^2 from positive to negative spontaneously

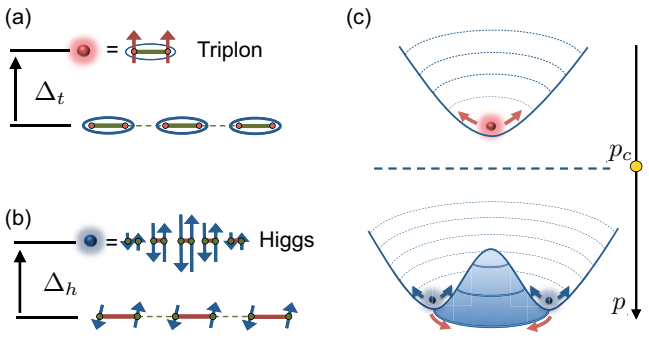

FIG. 2. (Color online) Excitations of a dimerized quantum antiferromagnet. (a) illustrates the triply degenerate gapped triplon excitations. (b) illustrates the gapped longitudinal (Higgs) excitation. (c) illustrates the quantum phase transition; the strength of the interactions in either phase is depicted by the steepness of the "well." Within the ordered phase, the "Mexican hat" potential has a flat direction which supports the gapless Goldstone excitations (red arrows). Precisely at the QCP (dashed line), all directions flatten: the Higgs and triplon excitations become gapless and noninteracting, i.e., asymptotically free.

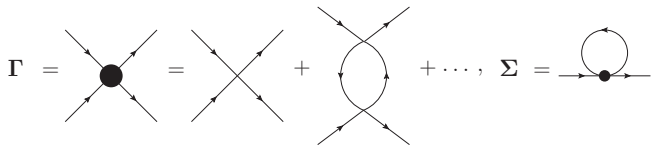

FIG. 3. Diagrams for the vertex Γ and self-energy Σ.

breaks the O(3) symmetry of the system. In the broken phase there are two gapless transverse (Goldstone [19]) excitations and one gapped longitudinal (Higgs) excitation. One easily recovers the known relation; Higgs gap/triplon gap $= \sqrt{2}$ [20], explicitly $\Delta_t(p) = m_0(p)$ and $\Delta_h(p) = \sqrt{2}|m_0(p)|$.

The above analysis does not account for quantum or thermal fluctuations. All fluctuations considered in the present Rapid Communication originate from the vertex and self-energy diagrams shown in Fig. 3. The vertex corrections result in the running coupling constant α_Λ (see, e.g., Ref. [10] or Supplemental Material Section A),

$$\alpha_\Lambda = \frac{\alpha_0}{1 + \frac{(N+8)\alpha_0}{8\pi^2} \ln(\Lambda_0/\Lambda)} . \tag{2}$$

Here Λ is the energy/momentum scale, Λ_0 is the normalization point, $\alpha_{\Lambda_0} = \alpha_0$, and $N = 3$ corresponds to O(3) spin symmetry of the system. Equation (2) has been obtained within the single-loop renormalization group, which implies that $\alpha_0/8\pi \ll 1$. At the same time the logarithmically enhanced denominator in (2) can be arbitrarily large. Note that the normalization point Λ_0 can be arbitrary; generally, it is not equal to the ultraviolet cutoff related to the lattice spacing. Equation (2) has a pole at $\Lambda = \Lambda_L = \Lambda_0 e^{8\pi^2/(N+8)\alpha_0}$. This is the famous Landau pole much debated in quantum field theory [3]. Remarkably, quantum magnets can shed light on the problem; we return to this point later. The running coupling constant at zero temperature versus pressure is plotted in Fig. 4. This curve is extracted from available experimental data. The coupling constant vanishes at the QCP, indicating

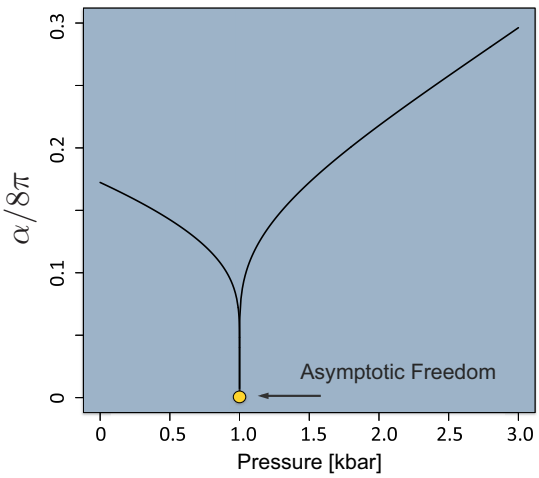

FIG. 4. (Color online) Zero-temperature running coupling constant vs pressure in $TlCuCl_3$. The constant vanishes at the QCP (yellow point).

the asymptotic freedom. Figure 4 represents one of our central results; below we explain how we obtain it.

At zero temperature, equations for the running mass and for the running staggered magnetization are well known [10] (see also Supplemental Material Sections B and C),

$$m^2(p,\Lambda) = \gamma^2(p_c - p)\left[\frac{\alpha_\Lambda}{\alpha_0}\right]^{\frac{N+2}{N+8}}, \tag{3}$$

$$\varphi_c^2(p,\Lambda) = \frac{\gamma^2(p-p_c)}{\alpha_0}\left[\frac{\alpha_0}{\alpha_\Lambda}\right]^{\frac{6}{N+8}}. \tag{4}$$

To find actual values of the gap in the disordered phase one has to solve Eq. (3) at $p < p_c$ with $\Delta_t = \Lambda = m$. To find the Higgs gap in the ordered phase one has to solve Eq. (3) at $p > p_c$ with $\Delta_H = \Lambda = \sqrt{2}|m|$. The relation $\Delta_H/\Delta_t = \sqrt{2}$ [20] remains valid with logarithmic accuracy.

We need to extend the theory to nonzero temperatures. Our goal is to find excitation spectra; therefore we cannot use the imaginary-time Matsubara technique. We need to work with real frequencies at a nonzero temperature. Generally, there is not a regular diagrammatic technique which allows us to calculate real-frequency Green's functions at nonzero temperature. Fortunately, in the present case such a calculation is possible within standard techniques. This possibility comes from the two following observations. (i) Multiloop logarithmic corrections are universal; they are not sensitive to whether frequency/energy is real or imaginary. (ii) The leading in α correction which contains powers of temperature comes only from the self-energy diagram shown in Fig. 3. Calculation of this diagram does not cause problems since, while it depends on temperature, it is frequency independent. Still, there is a minor complication related to point (ii). The complication is due to temperature broadening (quasiparticle lifetime) because of scattering from the heat bath of magnons. Below we explain how we address this issue. To be specific let us consider the triplon gap in the disordered phase. Calculation of the self-energy Σ (Fig. 3) gives the following answer (see Supplemental Material Section B):

$$\Delta_t^2(p,T,\Lambda) = \gamma^2(p_c - p)\left[\frac{\alpha_\Lambda}{\alpha_0}\right]^{\frac{N+2}{N+8}} + (N+2)\alpha_\Lambda \sum_{\mathbf{k}} \frac{1/\omega_{\boldsymbol{k}}}{e^{\frac{\omega_{\boldsymbol{k}}}{T}} - 1}. \tag{5}$$

At zero temperature the second term on the right-hand side is zero, and Eq. (5) becomes identical to Eq. (3). The value of the lower logarithmic cutoff in (5) is obvious, $\Lambda = \max\{\Delta_t, T\}$. The triplon dispersion is harder. The naive formula $\omega_{\boldsymbol{k}} = \sqrt{\boldsymbol{k}^2 + \Delta_t^2}$ is incomplete because at small $\boldsymbol{k}$ and close to the Néel temperature where $\Delta_t \to 0$ the line width Γ_t (temperature broadening) becomes larger than the gap. Physically, the inequality $\Gamma_t > \Delta_t$ is an indication of the dimensional crossover, $4D \to 3D$. Sufficiently close to the Néel temperature, critical indices take the 3D classical values. To resolve the problem we take $\omega_{\boldsymbol{k}} = \sqrt{\boldsymbol{k}^2 + \Delta_t^2 + \Gamma_t^2}$; this is a standard way to describe a damped harmonic oscillator (see, e.g., Ref. [11]). Of course, the modified dispersion is not sufficient to fully describe the dimensional crossover, but it is sufficient for the purposes of the present work. The line broadening we take directly from experiment, $\Gamma_t = \xi T$, where $\xi \approx 0.15$ [11]. Solution of Eq. (5) with $\Delta_t = 0$ gives the Néel temperature as a function of pressure $T_N(p)$.

One can also approach the Néel temperature from the ordered phase (see Supplemental Material Section C). In this case there are two Goldstone modes and one Higgs mode. The equation for the Higgs gap is similar to (5),

$$\Delta_H^2(p,T,\Lambda) = 2\left\{\gamma^2(p-p_c)\left[\frac{\alpha_\Lambda}{\alpha_0}\right]^{\frac{N+2}{N+8}} - (N-1)\alpha_\Lambda \times \sum_{\mathbf{k}} \frac{1/k}{e^{\frac{k}{T}} - 1} - 3\alpha_\Lambda \sum_{\mathbf{k}} \frac{1/\omega_{\boldsymbol{k}}}{e^{\frac{\omega_{\boldsymbol{k}}}{T}} - 1}\right\}. \tag{6}$$

Again, $\Lambda = \max\{\Delta_H, T\}, \omega_{\boldsymbol{k}} = \sqrt{\boldsymbol{k}^2 + \Delta_H^2 + \Gamma_H^2}$, and $\Gamma_H = \zeta T$. The Néel temperature determined from the condition $\Delta_t = 0$, Eq. (5), must be identical to that determined from $\Delta_H = 0$, Eq. (6). From here we conclude that broadening of the Higgs mode is larger than that of the triplon, $\zeta \approx 0.3$ compared to $\xi \approx 0.15$. The larger broadening is consistent with the data [11]. We note that the critical exponent of the magnetization in Eq. (4) is identical to that found for the Néel temperature by solving Eq. (5) or (6). This agrees with the latest quantum Monte Carlo simulations on the 3D dimerized antiferromagnet [21].

Now, we are fully armed to perform fits to experimental data. We set the normalization point $\Lambda_0 = 1$ meV. We remind the reader that this choice is arbitrary; one can always use a different normalization point with an appropriate rescaling of the coupling α_0. There are three fitting parameters, the critical pressure p_c, the coefficient γ^2 in the pressure dependence of the bare mass, and the coupling constant α_0. Points in Fig. 5(a) show experimental values of the triplon and Higgs gaps for various pressures at $T = 1.85$ K. Points in Fig. 5(b) show Néel temperatures for various pressures. The data are taken from Refs. [11–13].

Solid curves in both panels show fits of the data with Eqs. (2), (5), and (6). Values of the fitting parameters are

$$p_c = 1.01 \text{ kbar}, \quad \gamma = 0.68 \text{ meV/kbar}^{1/2}, \quad \frac{\alpha_0}{8\pi} = 0.23\,. \tag{7}$$

It is worth noting that while $T = 1.85$ K is a pretty low temperature, the temperature corrections in Eqs. (5) and (6) are not negligible. In the present work we set the triplon speed equal to unity. If one restores three different speeds along three different principal directions of the lattice, c_1, c_2, c_3, then Eq. (7) is changed to $\alpha_0/(8\pi c_1 c_2 c_3) = 0.23$. This value is close to the value $\alpha_0/(8\pi c_1 c_2 c_3) = 0.21$ obtained in Ref. [17] from the lifetime of the Higgs mode. Reference [17] did not account for the running coupling constant; however, experimentally, the major contribution to the lifetime data comes from Higgs magnons with energy of about 1 meV. This energy is taken as the normalization point in the present work. Coincidence of the energy scales explains the very close agreement between the accurate result of the present work and the approximate result of Ref. [17].

We stress that the coupling constant significantly changes along the fitting curves in Fig. 5. To illustrate this change we present Fig. 6, which shows how the constant runs

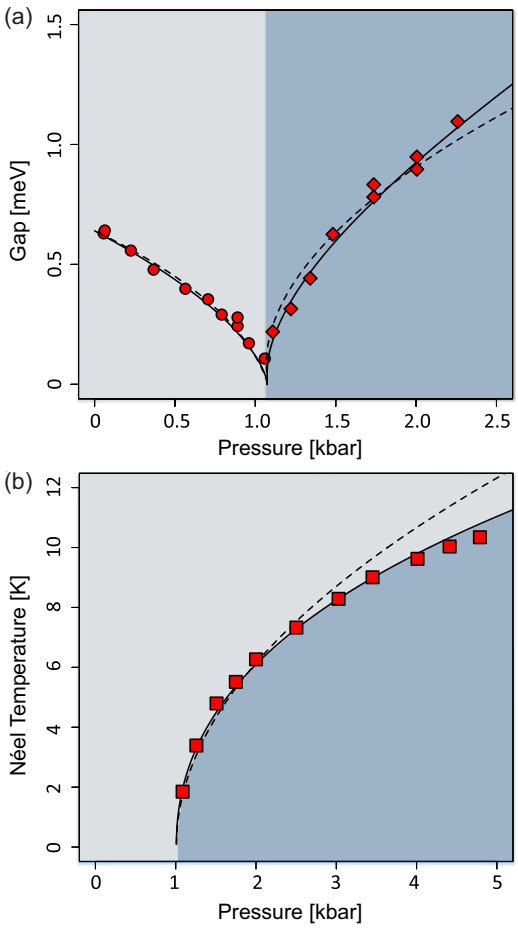

FIG. 5. (Color online) (a) Triplon and Higgs gaps vs pressure at temperature $T = 1.85$ K. Points show experimental data from Ref. [13]. (b) Néel temperature vs pressure. Points show experimental data from Ref. [12]. In both plots the solid and dashed curves are quantum field theory fits with and without accounting for the running coupling constant, respectively.

along the Néel temperature curve. Similar running is shown in Fig. 4, where the coupling constant is plotted versus pressure at zero temperature. In this case the infrared cutoff in Eq. (2) for α_Λ is equal to triplon/Higgs gap. The position of the Landau pole follows from the known value of the coupling constant, $\Lambda_L = \Lambda_0 e^{8\pi^2/11\alpha_0} \approx 3.5$ meV. This energy is higher than that of the experimentally studied regime and is comparable to the expected ultraviolet cutoff related to the dispersion along the third axis (see discussion in Ref. [17]). Experimental and theoretical studies in this energy range can shed light on Landau pole physics as well as the expected dimensional crossover in $TlCuCl_3$. Alternatively,

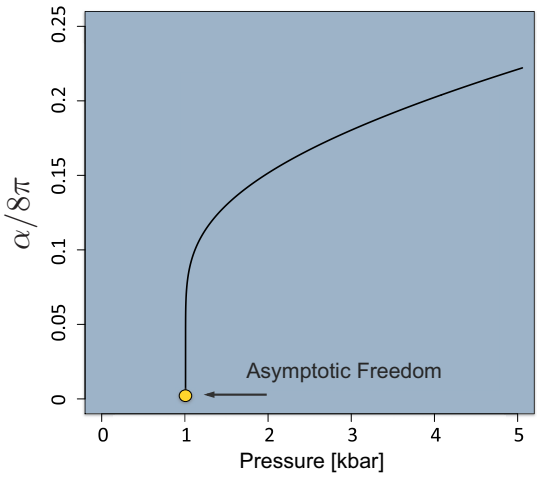

FIG. 6. (Color online) Running coupling constant vs pressure along the Néel temperature curve. Unlike Fig. 4 where the temperature is zero, in this case $T = T_N(p)$. According to Eqs. (5) and (6), the infrared cutoff in Eq. (2) for α_Λ is $\Lambda = T_N(p)$. The QCP is again marked by the yellow dot.

Landau pole physics can be addressed in quantum Monte Carlo studies of dimerized spin-lattice models [21,22]. In this case $\Lambda_L$can be smaller than the ultraviolet cutoff (inverse lattice spacing).

Our central goal is to pin down the running coupling constant which vanishes at the QCP giving rise to asymptotic freedom. To check this statement we also perform a fit of the data with a fixed coupling constant. We use the same Eqs. (5) and (6) but set $\alpha_\Lambda = \alpha_0$. Best-fit parameters become $p_c = 1.01$ kbar, $\gamma = 0.64$ meV/kbar$^{1/2}$, $\alpha_0/8\pi = 0.16$. Corresponding fitting curves are shown in Fig. 5 by dashed lines. It is seen from the quality of the fits that the running coupling plays a crucial role in describing the static properties of the system; the analysis clearly demonstrates the running coupling constant.

Asymptotic freedom is a prominent physical phenomenon. It is the remarkable experimental control of the quantum antiferromagnet $TlCuCl_3$ that has allowed the present work to identify the logarithmic decay of the coupling constant. More generally, with such remarkable experimental control, $TlCuCl_3$ and other quantum antiferromagnets provide an ideal playground for studies of the Landau pole physics and many other nontrivial quantum phenomena.

We thank B. Normand, A. Sandvik, and Y. Kharkov for many useful discussions. We also thank C. Rüegg for his comments regarding the decay widths. Research funded by the Australian Research Council DP110102123.

[1] D. J. Gross and F. Wilczek, Ultraviolet Behavior of Non-Abelian Gauge Theories, Phys. Rev. Lett. **30**, 1343 (1973).

[2] H. D. Politzer, Reliable Perturbative Results for Strong Interactions, Phys. Rev. Lett. **30**, 1346 (1973).

[3] L. D. Landau, A. A. Abrikosov, and I. M. Khalatnikov, The removal of infinities in quantum electrodynamics, Dokl. Akad. Nauk SSSR **95**, 497 (1954); An asymptotic expression of the electron Green function in quantum electrodynamics, **95**, 773

(1954); An asymptotic expression of the photon Green function in quantum electrodynamics, **95**, 1177 (1954).

[4] D. C. Elias, R. V. Gorbachev, A. S. Mayorov, S. V. Morozov, A. A. Zhukov, P. Blake, L. A. Ponomarenko, I. V. Grigorieva, K. S. Novoselov, F. Guinea, and A. K. Geim, Dirac cones reshaped by interaction effects in suspended graphene, Nat. Phys. **7**, 701 (2011).

[5] M. A. H. Vozmediano, Graphene: The running of the constants, Nat. Phys. **7**, 671 (2011).

[6] N. Motoyama, H. Eisaki, and S. Uchida, Magnetic Susceptibility of Ideal Spin 1/2 Heisenberg Antiferromagnetic Chain Systems, Sr_2CuO_3 and $SrCuO_2$, Phys. Rev. Lett. **76**, 3212 (1996).

[7] W. McRae and O. P. Sushkov, Magnetic moment of a spinon and thermodynamic properties of the one-dimensional Heisenberg model, Phys. Rev. B **58**, 62 (1998).

[8] H. Tanaka, K. Goto, M. Fujisawa, T. Ono, and Y. Uwatoko, Magnetic ordering under high pressure in the quantum spin system $TlCuCl_3$, Phys. B (Amsterdam, Neth.) **329–333**, 697 (2003).

[9] O. Nohadani, S. Wessel, and S. Haas, Quantum phase transitions in coupled dimer compounds, Phys. Rev. B **72**, 024440 (2005).

[10] J. Zinn-Justin. *Quantum Field Theory and Critical Phenomena* (Oxford University Press, Oxford, 2002).

[11] P. Merchant, B. Normand, K. W. Krämer, M. Boehm, D. F. McMorrow, and Ch. Rüegg, Quantum and classical criticality in a dimerized quantum antiferromagnet, Nat. Phys. **10**, 373 (2014).

[12] Ch. Rüegg, A. Furrer, D. Sheptyakov, Th. Strässle, K. W. Krämer, H.-U. Güdel, and L. Mélési, Pressure-Induced Quantum Phase Transition in the Spin-liquid $TlCuCl_3$, Phys. Rev. Lett. **93**, 257201 (2004).

[13] Ch. Rüegg, B. Normand, M. Matsumoto, A. Furrer, D. F. McMorrow, K. W. Krämer, H. U. Güdel, S. N. Gvasaliya, H. Mutka, and M. Boehm, Quantum Magnets Under Pressure: Controlling Elementary Excitations in $TlCuCl_3$, Phys. Rev. Lett. **100**, 205701 (2008).

[14] See Supplemental Material at http://link.aps.org/supplemental/10.1103/PhysRevB.92.220401 for detailed theoretical derivations, and a discussion of the influence of the spin-orbit anisotropy.

[15] S. Sachdev, in *Understanding Quantum Phase Transitions*, edited by L. D. Carr (Taylor and Francis, Boca Raton, FL, 2010).

[16] S. Sachdev, *Quantum Phase Transitions* (Cambridge University Press, Cambridge, 2011).

[17] Y. Kulik and O. P. Sushkov, Width of the longitudinal magnon in the vicinity of the O(3) quantum critical point, Phys. Rev. B **84**, 134418 (2011).

[18] J. Oitmaa, Y. Kulik, and O. P. Sushkov, Universal finite-temperature properties of a three-dimensional quantum antiferromagnet in the vicinity of a quantum critical point, Phys. Rev. B **85**, 144431 (2012).

[19] J. Goldstone, A. Salam, and S. Weinberg, Broken symmetries, Phys. Rev. **127**, 965 (1962).

[20] S. Sachdev, Exotic phases and quantum phase transitions: Model systems and experiments, arXiv:0901.4103.

[21] Y. Q. Qin, B. Normand, A. W. Sandvik, and Z. Y. Meng, Multiplicative logarithmic corrections to quantum criticality in three-dimensional dimerized antiferromagnets, Phys. Rev. B **92**, 214401 (2015).

[22] S. Jin and A. W. Sandvik, Universal Néel temperature in three-dimensional quantum antiferromagnets, Phys. Rev. B **85**, 020409(R) (2012).